Journal of Materials Chemistry B

Accepted Manuscript

ROYAL SOCIETY OF CHEMISTRY

www.rsc.org/materialsB

Journal Name

ARTICLE

Enhancing both CT imaging and natural killer cell-mediated cancer cell killing by a GD2-targeting nanoconstruct

Received 00th January 20xx,
Accepted 00th January 20xx

DOI: 10.1039/x0xx00000x

www.rsc.org/

Peifu Jiao,[a,b] Mario Otto,[c] Qiaohong Geng,[b] Chencan Li,[d] Faming Li,[b] Elizabeth R. Butch,[e] Scott E. Snyder,[e] Hongyu Zhou[a]* and Bing Yan[a]*

Although nanomaterials have been widely investigated for drug delivery, imaging and immunotherapy, their potential roles in triggering innate cellular immune responses while simultaneously serving as imaging enhancer remain unexplored. In this work, gold nanoparticles (GNPs) conjugated to the tumor-targeting anti-GD2 antibody hu14.18K322A, namely HGNPs, were designed and synthesized to specifically enhance computerized tomography (CT) imaging contrast and to stimulate the attack of neuroblastoma and melanoma cells by natural killer (NK) cells. The HGNPs specifically targeted GD2-positive neuroblastoma (NB1691) and melanoma (M21) cells, with an enhancement of CT contrast images of the HGNP-labeled cell pellets by 5.27- and 7.66-fold, respectively, compared to images of unlabeled cell pellets. The HGNPs also triggered NK-mediated antibody-dependent cellular cytotoxicity (ADCC) in NB1691 and M21 cells with a two-fold higher efficacy compared to that elicited by hu14.18K322A alone, with no adverse effect to GD2-negative PC-3 cells. These results suggest that HGNPs are promising theranostic agents for neuroblastoma and melanoma cancers.

1. Introduction

Early tumor detection is associated with an overall survival rate in cancer patients.[1-3] At the early stage of tumor development, tumors can be treated more effectively using non-invasive techniques besides chemotherapy, such as photothermal therapy,[4, 5] photodynamic therapy,[6] and hyperthermia therapy.[7] These methods usually result in good tumor inhibition with minor side effects to normal tissues. However, the early diagnosis of tumors remains a significant challenge. Even though computerized tomography (CT) is widely used as the standard imaging method in tumor diagnosis,[8] this method cannot detect tumors that are smaller than 0.5 cm in diameter.[9] Furthermore, CT is not able to distinguish between cancerous and benign tissues due to the lack of tumor-specific image-enhancing agents. As a result, very small primary or metastasized tumors cannot be detected by this modality.

Gold nanoparticles (GNPs) are growing as one of the most talent CT contrast agents because of the remarkable properties GNPs have, such as high X-ray absorption coefficient, outstanding biocompatibility, low cytotoxicity, unique surface plasmon resonance, and easy surface modification.[10, 11] The X-ray attenuation of gold nanoparticles (GNPs) is much higher than that of iodine-based contrast agents for CT at the same molar concentration.[12] Moreover, GNPs with tumor cell targeting molecules can specifically accumulate in the tumor tissues, leading to a fascinating feature of molecular imaging.[13-15] GD2 disialoganglioside is a carbohydrate antigen that is highly expressed in tumors of neuroectodermal origins, such as neuroblastoma, melanoma, brain tumors and certain sarcomas. In healthy tissues, GD2 expression is restricted to the brain, as well as select peripheral nerve fibers and melanocytes, which are inaccessible to circulating antibodies.[16-19] Therefore, GD2 is considered to be an ideal target for the specific imaging of GD2-positive tumors, with minimal harm to normal tissues.[20-22] Particularly, Ch14.18 (dinutuximab, Unituxin), achimeric anti-GD2 antibody, has recently been approved by the FDA as a first-line therapy for pediatric neuroblastoma patients through binding to GD2 molecules at cell surface and inducing cell lysis of GD2 expressing neuroblastoma cells through antibody-dependent cell-mediated cytotoxicity (ADCC).[23] However, systemic administration of ch14.18 is associated with partially morphine-resistant pain.[24-27] Hu14.18K322A is a clinical-grade, humanized version of ch14.18 that has an additional point mutation that markedly decreases antibody-mediated complement activation at peripheral nerve fibers, a process that plays a major role in anti-GD2 antibody

[a] School of Chemistry and Chemical Engineering, Shandong University, Jinan, Shandong 250100, China
[b] Department of Chemistry, Qilu Normal University, Jinan, Shandong 250013, China
[c] Department of Pediatrics, Division of Pediatric Hematology, Oncology and Bone Marrow Transplant, University of Wisconsin-Madison, Madison, WI 53705, USA
[d] TR Pharma & Tech Co., Ltd., Jinan, Shandong 250101, China.
[e] St. Jude Children's Research Hospital, Memphis, Tennessee 38105, USA.
*Corresponding authors: Professor Bing Yan, drbingyan@yahoo.com; Dr. Hongyu Zhou, hyzhou001@gmail.com
*Correspondence address - drbingyan@yahoo.com or byan992000@yahoo.com

therapy-induced allodynia.[24] Hu14.18K322A is currently under investigation in a phase II immunotherapy study for pediatric neuroblastoma patients at St. Jude Children's Research Hospital in the U.S.A.[28-30]

Although nanoconstructs have been explored for imaging enhancement, drug delivery applications and immunotherapy,[31, 32] their potential roles in triggering innate cellular immune responses while simultaneously serving as imaging enhancer remain unexplored. We hypothesize that when hu14.18K322A is conjugated to GNPs, in addition to its cancer cell-targeting ability, its Fc portion may convert natural killer (NK) cells to cancer cell killers after binding to the corresponding NK cell receptor,[33] and the NK cell-mediated cancer cell killing may be enhanced as a result of improved cellular binding and uptake, thus we can reach enhancing both CT imaging and NK cell-mediated cancer cell killing by a single GD2-targeting nanoconstruct. In this work, we designed and synthesized the nanoconstruct, in which hu14.18K322A is incorporated as a GD2-targeting and NK cell-activating moiety, with the gold core serving as a CT signal-enhancing agent. These hu14.18K322A-conjugated GNPs, namely HGNPs, specifically targeted GD2-positive neuroblastoma (NB1691) and melanoma (M21) cells, resulting in enhancing the CT imaging contrasts of these cell pellets. The HGNPs also triggered NK-mediated ADCC in NB1691 and M21 cells with no adverse effect on GD2-negative PC-3 cells.

2. Experimental section

2.1. Materials and reagents

All starting materials are obtained from commercial suppliers. The hu14.18K322A anti-GD2 antibody (provided by EMD Sorono) is produced for clinical and research use by Children's GMP, LLC (Memphis, TN). TEM images were captured using a JEOL 1200 EX transmission electron microscope (JEOL, Tokyo, Japan). ICP-MS measurements were performed using a Varian 820-MS spectrometer (Varian, Santa Clara, CA). Flow cytometry experiments were performed with a BD LSR II flow cytometer (Becton Dickinson, San Jose, CA, USA). Confocal microscopy experiments were performed using a Nikon Eclipse C1si spectral imaging confocal microscope system according to the manufacturer's instructions (Nikon Instruments, Melville, NY, USA). CT studies were performed using a Siemens Inveon micro-CT scanner (Siemens Medical Solutions).

2.2. Preparation of HGNPs

The hu14.18K322A antibody (1 mL, 8.6 mg/mL) was washed three times with activation buffer (0.1 M MES, 0.5 M NaCl, pH = 6.0) and re-dissolved in 8 mL of activation buffer at 4℃. EDC (10 mg) and sulfo-NHS (25 mg) in 2 mL of activation buffer were added to the antibody solution. The mixture was stirred for 20 minutes at room temperature and filtered using a centrifugal filter (10,000 MWCO) at 4℃ to remove excess activation agents. The activated antibody was stirred with cysteine (5 mg) in 10 mL of PBS for 2 hours at 4℃ and washed three times with Milli-Q water to remove excess cysteine. The retained Cys-antibody was re-dissolved in 10 mL of Tween80 solution (0.03%) and added to the GNP (15 nm) solutions. The mixture was then stirred for 24 hours at 4℃. HS-PEG_{5000} (3 mg) in 1 mL of Milli-Q water was added. The obtained HGNP solution was stirred for another 24 hr at 4℃ and washed three times with PBS to remove excess HS-PEG_{5000}.

2.3. Cell culture

PC-3 cells were maintained in ATCC-formulated F-12K medium supplemented with 10% fetal bovine serum (FBS) and 1% penicillin-streptomycin. M21 and NB1691cellswere maintained in RPMI-1640 medium supplemented with 10% FBS and 1% penicillin-streptomycin. Cells were cultured in a 5% CO_2 humidified incubator at 37 ℃. All cell lines used in this study were prior to passage 40.

2.4. GD2 expression by flow cytometry

Targeted binding of hu14.18K322A to the GD2 antigen was assessed by flow cytometry. The cell lines used for this experiment were GD2-positive neuroblastoma cell line NB1691and melanoma cell line M21. The GD2-negative human prostate carcinoma line PC-3 was used as a negative control. In brief, cultured cells were trypsinized and resuspended in culture medium to inactivate trypsin. The cells ($1x10^6$) were dispensed into 5-mL tubes and washed twice with ice-cold staining buffer (PBS containing 1% heat-inactivated FBS, both from Invitrogen, Carlsbad, CA, USA, and 0.05% sodium azide, Sigma-Aldrich, St. Louis, MO). The cell pellets were resuspended in 200 µL of staining buffer, and 20 µL of either hu14.18K322A (5 µg/mL) was added. The samples were incubated for 30 minutes on ice, washed three times with washing buffer (0.05% sodium azide in PBS with 3% normal goat serum), and resuspended in 100 µL of staining buffer. Ten microliters of APC mouse anti-human IgG (BD Pharmingen, San Diego, CA, USA) was added to all samples, and the cells were incubated for 30 minutes in the dark on ice, washed three times with washing buffer and resuspended in 200 µL of staining buffer. Fifty microliters of DAPI (1 µL/mL, 4, 6-diamidino-2-phenylindoledihydrochloride, Molecular Probes, Eugene, OR, USA) solution was added to discriminate non-viable cells. Data files were collected using a BD LSR II flow cytometer (Becton Dickinson, San Jose, CA, USA). A minimum of $1x10^5$ live cells were collected for each tube, and the results were analyzed using BD FACSDiva Software (Becton Dickinson).

2.5. Dark-field microscopy

Cells were incubated with HGNPs in their corresponding culture medium. After 12 hr incubation, the cell samples were rinsed with DPBS and fixed with 4% paraformaldehyde or ethanol for 20-30 minutes. Dark-field microscopy images were captured using a Nikon E800 microscope and a dry dark-field condenser (NA 0.95-0.8).

2.6. Transmission electron microscopy

Cells were incubated with HGNPs in the appropriate cell culture medium for 4 or12 hr. The samples were washed twice with DPBS, and attached cells were fixed with 2.5% glutaraldehyde in 0.1 M Na-cacodylate buffer (Tousimis Research Corporation) for 20-30 min at room temperature. After fixation, the cell samples were washed twice with DPBS. Ultrathin sample sections were examined using a JEOL 1200 EX transmission electron microscope (JEOL, Tokyo, Japan).

2.7. Confocal microscopy

To determine the specific binding of HGNPs to surface GD2, M21 melanoma cells were grown in culture media on poly-*D*-lysine-coated 35-mm glass-bottom culture dishes (MatTek, Ashland, VA, USA) until 80% confluency. The GD2-negative prostate carcinoma cell line PC-3 was used as a negative control. The cells were washed twice with DPBS and fixed in 4% formaldehyde (Polysciences, Warrington, PA, USA) for 10 minutes at room temperature. The formaldehyde was removed, and fixation was stopped by washing three times with DPBS (Invitrogen) for 2 minutes and subsequently rinsing three times with DPBS (1X) for 5 minutes. The cells were incubated with DPBS containing 1% BSA for 10 minutes (blocking) and then incubated with either hu14.18K322A (80 nM) or HGNPs (GNP concentration: 5 nM, IgG concentration: 80 nM) in DPBS or without primary antibody for 12 hr in the dark at ambient temperature. After washing three times with DPBS, the cells were incubated with goat-anti-human IgG Alexa Fluor 488 (Invitrogen, 80 nM) in DPBS for 1 hour in the dark at ambient temperature. The cells were rinsed three times with DPBS, and the ProLong® antifade reagent with DAPI mounting medium (Invitrogen) was applied and allowed to cure for 24 hours in the dark. Confocal microscopy was performed using a Nikon Eclipse C1si spectral imaging confocal microscope system according to the manufacturer's instructions (Nikon Instruments, Melville, NY, USA).

2.8. ICP-MS experiments

The obtained HGNPs (100 mL) were centrifuged at 25,000 rpm for 1 hour, washed with PBS (pH = 7.4), and dissolved in 10 mL PBS to obtain an HGNP stock solution. The concentration of the stock solution was measured by ICP-MS. All cells were cultured in 12-well plates at 20,000 cells/well. After the cells reached 70% confluency, HGNPs in medium were added. The cells were incubated in a 5% CO_2 humidified incubator at 37°C, and the samples including floating cells were harvested, and washed with DPBS (1 mL × 3). The harvested cells were resuspended in 500 µL of medium and counted using a Cellometer® Auto T4 cell counter (Nexcelom Bioscience). Cell samples (400 µL) were incubated with 400 µL of Aqua Regia at 37°C and centrifuged after 12 hr. The supernatant (500 µL) was diluted to 5mL with a 50 ppb 236Y internal standard solution in 1% HNO_3 and used for ICP-MS measurements. A series of gold standard solutions (1000, 500, 250, 100, 50, 10, 5, and 1 ppb) with 50 ppb 236Y internal standard were prepared before each measurement. The resulting calibration curve was used to calculate the amount of gold taken up by different cells.

2.9. Competition experiment with free hu14.18K322A

M21 cells were plated in 12-well plates at 20,000 cells/well and grown to 70% confluency. Free hu14.18K322A (1, 5, 25, 100, and 200 nM; molecular weight of hu14.18K322A: 150 kD) was added to each sample and incubated for 4 hours at room temperature. HGNPs in cell culture medium (5 nM) were added and incubated for 12 hours at room temperature. The samples were harvested and washed three times with DPBS, and the harvested cells were counted using a Cellometer® Auto T4 cell counter (Nexcelom Bioscience). The harvested cell samples (400 µL) were treated with 400 µL of Aqua Regia at 37℃ for 12 hours and centrifuged at 1000 rpm for 5 minutes. The supernatant (500 µL) was used for ICP-MS measurements.

2.10. Cytotoxicity of HGNPs

HGNP-treated and control cells were cultured for 12 hours in 96-well plates in a 5% CO_2 humidified incubator at 37℃. The tested concentrations of HGNP were 0.1, 1, and 10 nM in the appropriate cell culture medium. After exposure, the HGNPs were removed, and 100 µl of fresh medium was added. Ten microliters of HGNP-treated and control cells were used for WST-1 cell proliferation assays (Roche Applied Science). The samples were shaken thoroughly for 1 minute before each measurement, and the absorbance of all samples was measured at 450 and 650 nm for HGNP and control cells, respectively, using a SpectraMax M5 microplate reader (Molecular Devices Sunnyvale, CA).

2.11. In Vitro CT imaging experiments

Target cells (M21and PC-3) were cultured in 75-cm^3 tissue culture flasks until 80-90% confluency was obtained. The medium was removed, and the cells were incubated for 12 hr in fresh culture medium containing HGNPs at a concentration of 5 nM. Control cells were incubated in medium without HGNPs.

After 12 hours, the medium was removed, and adherent cells were washed three times with PBS to remove unbound HGNPs. The cells were then trypsinized, washed three times with cell culture medium, counted and pelleted at 1000 rpm for 5 minutes in 1.5-mL conical tubes (Sarstedt, Newton, NC, USA).

CT studies were performed using a Siemens Inveon micro-CT scanner (Siemens Medical Solutions) with data acquired at an isotropic resolution of 107 µm. Briefly, the field of view (FOV) was set at 2048 x 3072 pixels with 180 projections throughout a full rotation (2 x averages per projection) and an acquisition time of 400 ms per projection (Binning x 2).

2.12. Antibody-dependent cellular cytotoxicity (ADCC) assay

2.12.1. Isolation of natural killer cells for the ADCC assay

Human peripheral blood mononuclear cells (PBMCs) from healthy adult donors were collected at St. Jude Children's Research Hospital using a protocol approved by the St. Jude Hospital Institutional Review Board. Natural killer cells were isolated from PBMCs using a direct magnetic labeling system for the isolation of CD56+ cells with subsequent enrichment on an AutoMACS device (Miltenyi Biotech, Auburn, CA). The CD56 antigen is expressed by most NK cells and a minor T cell subset (CD3+CD56+ natural killer T cells). Labeling and enrichment were performed according to the manufacturer's instructions. After isolation, the cells were incubated in culture medium supplemented with 50 IU/mL of IL-2 in a concentration of 2 x 10^6 cells/mL, as specified above, and allowed to recover for approximately 16-20 hours.

2.12.2. Antibody-dependent cellular cytotoxicity (ADCC) assay

ADCC was measured using a conventional two-hour europium-TDA (EuTDA) assay (Perkin-Elmer Wallac, Turku, Finland). Briefly, targeted cells were labeled with a hydrophobic fluorescence-enhancing ligand (BATDA) according to the manufacturer's instructions. Under basal conditions, intracellular hydrolysis of ester

bonds renders the ligand hydrophilic, and BATDA is unable to pass through the cell membrane. Cytolysis results in the release of ligand from the cytosol into the supernatant, where it reacts with europium to form a stable, fluorescent chelate. Labeled target cells were incubated for 4 hr in a 96-well plate: 5 x 10^3/well at 37°C in a 5% CO_2 atmosphere and 95% humidity with an NK-to-cancer cell ratio of 10:1, 5:1 and 1:1 in triplicate, with or without 3.3 nM of hu14.18K322A or 0.2 nM of HGNPs (hu14.18K322A content: 3.3 nM). ADCC elicited by NK cells from 4 different donors were isolated and tested. Following incubation, the supernatant was allowed to react with the europium solution, and time-resolved fluorescence was measured using a Perkin-Elmer Wallac Victor 2 device. Spontaneous release was determined by incubating the target cells in culture medium without NK cells. Maximal release was determined by adding 20 µL of a 1:10 dilution of Triton X-100 (Sigma-Aldrich) to dedicated wells containing target cells for the duration of the incubation period.

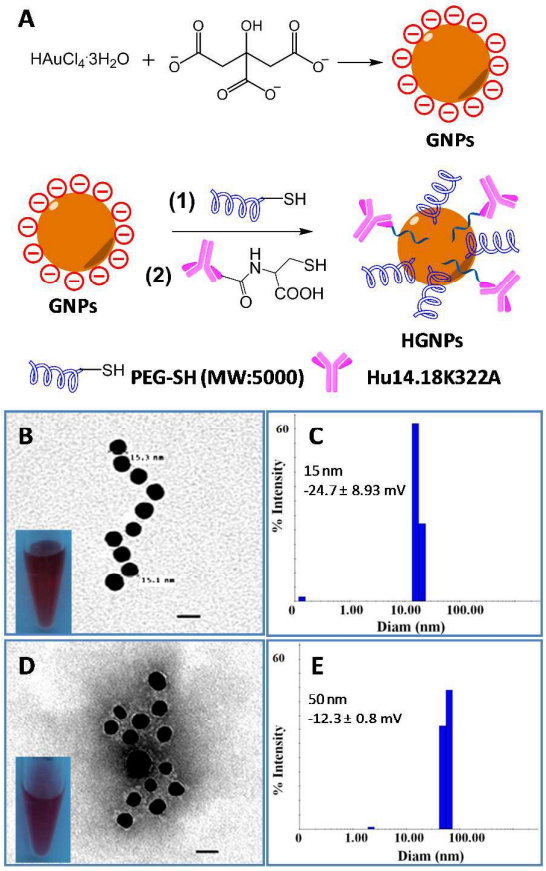

Fig. 1 Synthesis and characterization of HGNPs. A) Synthesis of GNPs and HGNPs. B) Transmission electron microscopy (TEM) image of GNPs (scale bar: 20 nm) and photograph of the GNP solution. C) The hydrodynamic diameter of GNPs analyzed by dynamic light scattering (DLS). D) TEM image of HGNPs (stained with 2% phosphotungstic acid, pH = 6.0, scale bar: 20 nm) and photograph of the HGNP solution. E) The hydrodynamic diameter of HGNPs obtained by DLS analysis.

3. Results and discussion

3.1. Synthesis and characterization of hu14.18K322A-functionalized GNPs (HGNPs)

Cancer-targeted moieties are considered essential tools for the early diagnosis of primary and metastasized microscopic tumors as well as for tumor-specific immunotherapy. To design a nanoconstruct that could combine these crucial properties for the GD2-positive malignancies neuroblastoma and melanoma, we conjugated the novel humanized anti-GD2 antibody hu14.18K322A to GNPs (**Fig. 1A and Fig. S1, ESI**). The antibody serves as a tumor cell-targeting and NK cell-engaging moiety, and the GNPs serve as CT-enhancing agents suitable for molecular imaging.[9] To avoid unspecific immunogenicity and to potentially enhance blood circulation time *in vivo*, we also incorporated PEG_{5000} groups into the hu14.18K322A-functionalized GNPs (HGNPs).[34] The as-synthesized GNPs had good water solubility. The diameter of the GNPs core was approximately 15 nm, as measured by TEM (**Fig. 1B**), which was consistent with the result from dynamic light scattering analysis (**Fig. 1C**). After conjugation with hu14.18K322A, Phosphotungstic acid staining of the HGNPs revealed gray clouds surrounding gold cores, indicating the binding of hu14.18K322A and PEG polymers to the nanoconstructs (**Fig. 1D**). The hydrodynamic diameter of the HGNPs in water was approximately 50 nm (**Fig. 1E**). As it has been shown that 50-nm nanoparticles demonstrate the greatest effect in binding to and the activation of membrane receptors,[35] HGNPs should exhibit great tumor and NK cell recognition. HGNPs had a zeta-potential of -12.3 mV compared with -24.7 mV for GNPs, indicating the successful conjugation of PEG_{5000} and hu14.18K322A antibody to GNPs. The evidence for antibody conjugation and the number of hu14.18K322A molecules per HGNP was quantitatively analyzed by elemental analysis of the nitrogen content in HGNPs.[36] There were approximately 16 antibody molecules conjugated to each HGNP particle.

3.2. GD2-dependent cytoselective internalization of HGNPs

We next tested whether HGNPs could selectively bind to GD2-positive tumor cells. Both neuroblastoma NB1691 and melanoma M21 cells had overexpression of the GD2 antigen, as determined by flow cytometry (**Fig. S2, ESI**). They were investigated in this work for cancer cell-specific targeting, while PC-3 cells did not express the GD2 antigen and were used as the negative control. HGNPs stock solution was made with an Au concentration of 2100 µg/mL as determined by ICP-MS. This concentration was converted to a molar concentration of 100 nM of HGNPs considering the density of Au and the average diameter of HGNPs.[37]

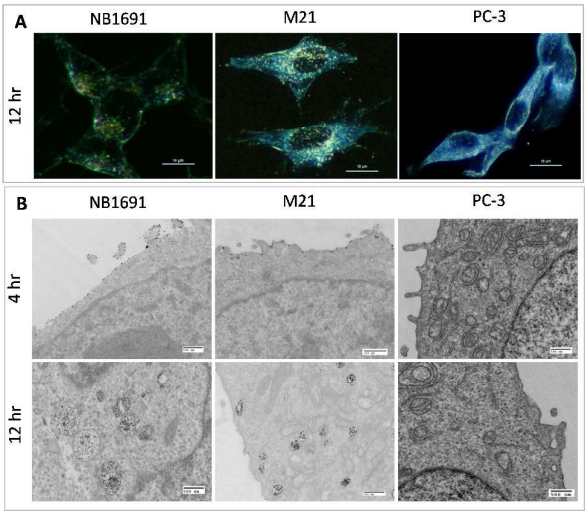

Fig. 2. GD2-dependent cell binding and internalization of HGNPs. A) Dark field images of NB1691, M21, PC-3 cells after incubation with HGNPs at 5 nM for 12 hr. The scale bar represents 10 μm. B) TEM images of NB1691, M21, PC-3 cells after incubation with HGNPs at 5 nM for 4 hr and 12 hr. The scale bar represents 500 nm.

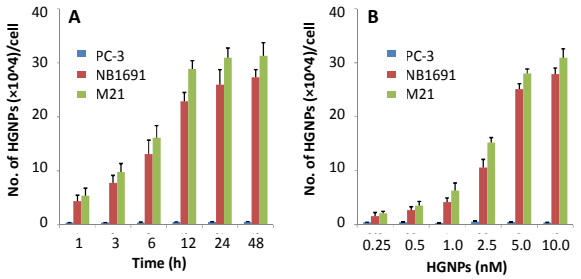

Fig.3 Quantitative analysis of HGNPs. A) Time-dependent binding and internalization of HGNPs (5 nM) inPC-3, NB1691, and M21 cells quantified by ICP-MS. B) Dose-dependent binding and internalization of HGNPs (12 hr) in PC-3, NB1691, and M21 cells.

We used several techniques to investigate cancer-specific targeting by HGNPs. The cellular binding and uptake of HGNPs was firstly determined by dark-field microscopy, Which clearly showed HGNPs in NB1691 and M21 cells after 12 h incubation at 37 ℃, while no HGNPs were found in PC-3 cells (**Fig. 2A**). The TEM images of NB1691 and M21 cells showed that most HGNPs bound to the cell surface at 4 hr and were heavily internalized and accumulated in endosome-like vehicles at 12 hr (**Fig. 2B**). For comparison, the PC-3 cells showed neither surface-bound nor internalized HGNPs (**Fig. 2B**). When a secondary antibody, goat-anti-human IgG Alexa Fluor 488, was used to mark the HGNPs in cells, these results were corroborated by confocal microscopy (**Fig. S3, ESI**). Internalized HGNPs were found to be mainly located in vesicle-like organelles in the cytoplasm, suggesting that they were likely internalized by GD2 binding-mediated endocytosis.

Quantitative assessment of GD2 binding and cell internalization of the HGNPs was performed using inductively coupled plasma mass spectrometry (ICP-MS). When the cells were incubated with 5 nM HGNPs, binding and internalization by $GD2^+$ tumor cells was increased with time and reached an equilibrium at 12 hr (**Fig. 3A**). For the control PC-3 cells, only a negligible amount of HGNPs were internalized. We then fixed the incubation time as 12 hr and cells were incubated with HGNPs at various concentrations, the maximal internalization of HGNPs by $GD2^+$ tumor cells was achieved at an HGNP concentration of 5 nM (**Fig. 3B**). Quantitative analysis revealed that the amounts of HGNPs internalized by NB1691 and M21 cells were 45-fold or 56-fold higher than that internalized by PC-3 cells at 12 hr, respectively, indicating a very high selectivity of HGNPs for neuroblastoma and melanoma cells. To reach the maximal HGNP internalization and selectivity, we used 5 nM as the HGNP concentration in the following experiments.

3.3. Inhibition of HGNP internalization in M21 Cells by free hu14.18K322A

To verify whether the specific targeting of neuroblastoma and melanoma cells by HGNPs was actually mediated by the GD2-receptor, we examined cell binding and internalization in M21 cells, which were pre-treated with free hu14.18K322A antibody. Competition of free antibody molecules for GD2 antigens on the cell surface considerably inhibited the binding of HGNPs to tumor cells (**Fig. 4**) TEM images showed a large amounts of HGNPs or HGNPs aggregates in M21 cells or on cell surface without free antibody pre-treatment (**Fig. 4A**), while only few HGNPs were found on cell membrane or inside M21 cells in presence of 5 nM of free hu14.18K322A (**Fig. 4B**). Quantitative ICP-MS analysis showed that free antibody molecules prevented internalization of HGNPs in a dose-dependent manner, with approximately 78% of inhibition at a free antibody concentration of 5 nM. These results confirm that HGNPs specifically target cancer cells through GD2 recognition and binding, while the absence of such binding on PC-3 cells is due to the lack of GD2 antigens on these cells.

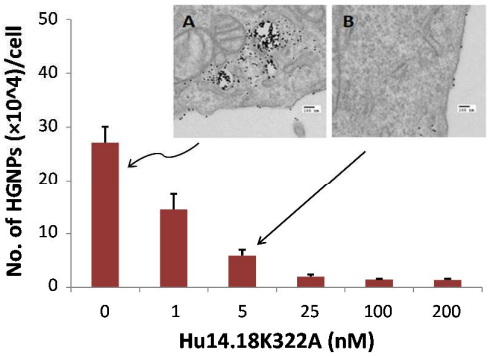

Fig. 4. Inhibition of HGNP binding and internalization by hu14.18K322Ain M21 cells. M21 cells were pretreated with hu14.18K322A at the indicated concentrations for 4 hr then treated with HGNPs at 5 nM for another 12 hr. The bound or internalized HGNPs were quantified by ICP-MS. Inset A shows a TEM image of an M21 cell pretreated with only cell culture medium following by treated with HGNPs at 5 nM for 12 hr. Inset B shows a TEM image of an M21 cell pretreated with 5 nM of hu14.18K322A following by treated with 5 nM of HGNPs for 12 hr. The scale bars in the insets are 100 nm.

3.4. *In vitro* cancer-specific CT imaging enhancement

The capability of HGNPs to specifically target the GD2 antigen provided us with an opportunity to selectively enhance the CT contrast of cancer cells *in vitro* and to kill cancer cells without harming normal cells that do not express GD2. Although the use of GNPs to enhance CT imaging for early tumor detection has been shown by other research groups,[38-40] there is still no report on using GNP-antibody conjugates for both CT and cancer cell killing by involving NK Cells. With this in mind, we first tested whether HGNP-targeted tumor cells demonstrate enhanced CT contrast *in vitro*. After incubating HGNPs with PC-3, NB1691, and M21 cells for 12 hr, no enhancement was observed for the image of the PC-3 cell pellet (1.06-fold, calculated by Image J). However, the contrast of the NB1691 and M21 cell pellets was enhanced by 5.27- and 7.66-fold, respectively (calculated by Image J), compared with that of the cell pellets without HGNPs (**Fig. 5**). This result demonstrated proof of principle that HGNPs targeted to tumor cells were able to significantly enhance the contrast of CT imaging in *ex vivo* phantom experiments simulating very small tumor volumes. If specific contrast agents were available, molecular CT imaging would be a powerful modality for the diagnosis of very small primary or metastasized tumors. Although our *in vitro* data are highly encouraging, further studies are needed to address whether systemically administered HGNPs could accumulate to sufficient amounts in tumors *in vivo* to enhance CT contrast versus imaging without or with iodine-based contrast agents.

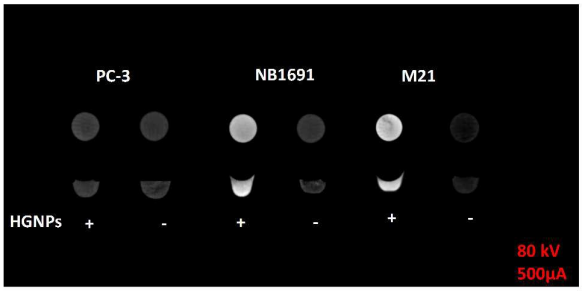

Fig. 5. CT images of PC-3, NB1691 and M21 cell pellet phantoms. Cells were treated with (+) or without (-) HGNPs (5 nM) in cell culture medium for 12 hr. Unbound HGNPs were removed by rigorous washing, three times with PBS.

3.5. HGNP-provoked antibody-dependent cellular cytotoxicity of cancer cells involving NK Cells

HNGPs were assembled via the random conjugation of hu14.18K322A to GNPs to create an HGNP construct in which the antibodies attached to the nanoparticles are fully functional, such that they recognize the GD2 antigen via an intact Fab fragment and are capable of eliciting antibody-dependent cytotoxicity via a functional Fc portion that is readily recognized by a receptor on the surface of NK cells.

NK cells are a type of innate cytotoxic lymphocyte critically involved in the defence against cancer cells. NK cells can identify target cells if they express certain stress signals, particularly if they lack or have down-regulated MHC class I expression or lack inhibitory ligands, as well as through a variety of other intricate recognition patterns.[41] NK cells also express CD16 (FcγRIII) receptors that recognize the Fc portion of antibodies.[42] When CD16 molecules on the NK cell surface bind to the Fc region of an antibody that is bound to a target cell via its Fab fragment, the NK cell releases cytokines such as granzymes, perforins, and interferon-γ (IFN-γ). These cytokines effectively kill cancer cells (**Fig. 6A**).[41, 43-45] This important immune response is termed antibody-dependent cellular cytotoxicity (ADCC), which is increasingly being exploited in tumor-targeted immunotherapies. We believe that when hu14.18K322A is conjugated to GNPs, the NK cell-mediated cancer cell killing would be enhanced as a result of improved cellular binding and uptake (**Fig. 6A**), so that we can reach enhancing both CT imaging and NK cell-mediated cancer cell killing by a single GD2-targeting nanoconstruct. Thus, we next tested whether HNGPs can indeed elicit NK cell-mediated ADCC.

Without the addition of NK cells, the HGNPs did not show any measurable cytotoxicity toward PC-3, NB1691 or M21 cells at concentrations up to 10 nM in a standard 12-hr cytotoxicity assay (**Fig. S4, ESI**). This result agrees with the opinion that surface-modified GNPs are biocompatible theranostic agents.[34, 46] However, when combined with NK cells, the HGNPs induced significant ADCC toward NB1691 and M21 cells (GD2-positive cells), as expected no ADCC toward PC-3 cells (GD2 negative) was observed at a very low effector-to-target (E:T) ratio of 1:1 (**Fig. 6B**). This strong ADCC effect was confirmed at higher E:T ratios of 5:1 (**Fig. 5C**) and 10:1 (**Fig. S5,**

ESI), and target cell killing reached almost 100%, comparable to the ADCC elicited by hu14.18K322A alone at the latter E:T ratios. Surprisingly, at the low E:T ratio of 1:1, the HGNPs elicited increased ADCC of NK cells toward target cells when compared to hu14.18K322A alone in equivalent molar concentrations. Specific lysis was 1.9-fold and 2.1-fold higher than that achieved with hu14.18K322A, indicating that antibodies conjugated to GNPs are capable of increasing the cytotoxic capacity of NK cells with regard to killing target cells. Multiple possible mechanisms exist, including increased chemokine release, steric advantages, or the binding of several NK cells simultaneously to a single cancer cell. Although the detailed mechanisms need to be elucidated, these results indicate that HGNPs hold great promise as a CT imaging enhancer and an effective agent for immunotherapy of GD2-positive malignancies such as neuroblastoma and melanoma. Further investigations will be aimed at the *in vivo* testing of HGNPs in preclinical models of these particularly deadly malignancies.

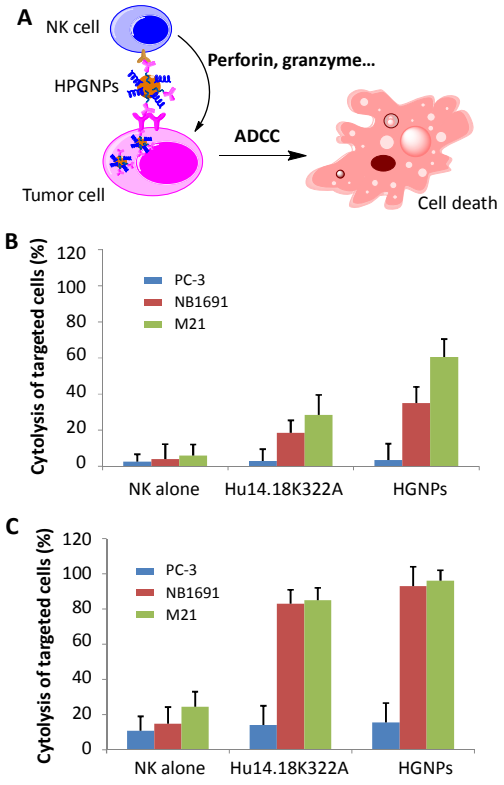

Fig. 6. Antibody-dependent cytotoxicity of NK cells toward PC-3, NB1691 or M21 cells. A) Schematic illustration of HGNPs stimulating the attacks on GD2 positive cells by NK cells and inducing immune-mediated cancer cell killing through ADCC. B, C). Cytotoxicity of HGNPs in present of NK cells. Cells were incubated with NK cells with hu14.18K322A or HGNPs at equivalent hu14.18K322A concentration of 3.3 nM for 4 hr. The ratio of NK cells to PC-3, NB1691 or M21 cells was 1:1 in B) and 5:1 in C).

4. Conclusions

There is an ever-increasing demand for the early detection of microscopic tumors, and improving tumor-targeting immunotherapeutic approaches is promising for reducing long-term toxic side effects. To fulfil these unmet clinical needs, novel tumor-specific agents need to be developed. In this work, we designed and synthesized a nanoconstruct, HGNPs, in which hu14.18K322A is incorporated as a GD2-targeting and NK cell-activating moiety, with the gold core serving as a CT signal-enhancing agent. The HGNPs specifically targeted neuroblastoma and melanoma cells and significantly enhanced CT imaging contrast of cell pellets in phantom experiments. Furthermore, the HGNPs were capable of inducing immune-mediated cancer cell killing through ADCC. This cancer-specific theranostic nanoconstruct shows great promise for improving the early diagnosis and treatment of GD2-positive tumors, and future pre-clinical studies with this novel construct will be aimed at translating our findings into clinical applications.

Acknowledgements

We thank Dr. Christopher Calabrese for help with CT phantom imaging acquisition and analysis. This work was supported by the National Natural Science Foundation of China (21137002 and 91543204), the Strategic Priority Research Program of the Chinese Academy of Sciences (XDB14030401), the Shandong Province Natural Science Foundation (ZR2013BQ010), and research grants from the American Lebanese Syrian Associated Charities (ALSAC).

Notes and references

1. R. Etzioni, N. Urban, S. Ramsey, M. McIntosh, S. Schwartz, B. Reid, J. Radich, G. Anderson and L. Hartwell, *Nat. Rev. Cancer*, 2003, **3**, 243-252.
2. S. C. Hiom, *Brit. J. Cancer*, 2015, **112**, S1-S5.
3. B. K. Edwards, E. Ward, B. A. Kohler, C. Eheman, A. G. Zauber, R. N. Anderson, A. Jemal, M. J. Schymura, I. Lansdorp-Vogelaar, L. C. Seeff, M. van Ballegooijen, S. L. Goede and L. A. G. Ries, *Cancer*, 2010, **116**, 544-573.
4. C. Ayala-Orozco, C. Urban, M. W. Knight, A. S. Urban, O. Neumann, S. W. Bishnoi, S. Mukherjee, A. M. Goodman, H. Charron, T. Mitchell, M. Shea, R. Roy, S. Nanda, R. Schiff, N. J. Halas and A. Joshi, *ACS Nano*, 2014, **8**, 6372-6381.
5. X. Huang, P. K. Jain, I. H. El-Sayed and M. A. El-Sayed, *Lasers Med. Sci.*, 2008, **23**, 217-228.
6. D. K. Chatterjee, L. S. Fong and Y. Zhang, *Adv. Drug Delivery Rev.*, 2008, **60**, 1627-1637.
7. A. K. Parchur, A. A. Ansari, B. P. Singh, T. N. Hasan, N. A. Syed, S. B. Rai and R. S. Ningthoujam, *Integr. Biol.*, 2014, **6**, 53-64.
8. D. Lardinois, W. Weder, T. F. Hany, E. M. Kamel, S. Korom, B. Seifert, G. K. von Schulthess and H. C. Steinert, *N. Engl. J. Med.*, 2003, **348**, 2500-2507.
9. R. Popovtzer, A. Agrawal, N. A. Kotov, A. Popovtzer, J. Balter, T. E. Carey and R. Kopelman, *Nano Lett.*, 2008, **8**, 4593-4596.

10. D. Kim, S. Park, J. H. Lee, Y. Y. Jeong and S. Jon, *J. Am. Chem. Soc.*, 2007, **129**, 7661-7665.
11. D. Xi, S. Dong, X. Meng, Q. Lu, L. Meng and J. Ye, *RSC Advances*, 2012, **2**, 12515-12524.
12. J. F. Hainfeld, D. N. Slatkin, T. M. Focella and H. M. Smilowitz, *Br. J. Radiol.*, 2006, **79**, 248-253.
13. P. Ghosh, G. Han, M. De, C. K. Kim and V. M. Rotello, *Adv. Drug Delivery Rev.*, 2008, **60**, 1307-1315.
14. M. De, P. S. Ghosh and V. M. Rotello, *Adv. Mater.*, 2008, **20**, 4225-4241.
15. E. Boisselier and D. Astruc, *Chem. Soc. Rev.*, 2009, **38**, 1759-1782.
16. G. Schulz, D. A. Cheresh, N. M. Varki, A. Yu, L. K. Staffileno and R. A. Reisfeld, *Cancer Res.*, 1984, **44**, 5914-5920.
17. L. Svennerholm, K. Bostrom, P. Fredman, B. Jungbjer, A. Lekman, J. E. Mansson and B. M. Rynmark, *BBA-Mol. Cell Biol. L.*, 1994, **1214**, 115-123.
18. K. Mujoo, D. A. Cheresh, H. M. Yang and R. A. Reisfeld, *Cancer Res.*, 1987, **47**, 1098-1104.
19. M. Ahmed and N.-K. V. Cheung, *FEBS Lett.*, 2014, **588**, 288-297.
20. M. Suzuki and N.-K. V. Cheung, *Expert Opin. Ther. Tar.*, 2015, **19**, 349-362.
21. D. C. Baiu, N. S. Artz, M. R. McElreath, B. D. Menapace, D. Hernando, S. B. Reeder, C. Gruettner and M. Otto, *Nanomed.*, 2015, **10**, 2973-2988.
22. Y. Xu, D. C. Baiu, J. A. Sherwood, M. R. McElreath, Y. Qin, K. H. Lackey, M. Otto and Y. Bao, *Journal of Materials Chemistry B*, 2014, **2**, 6198-6206.
23. U.S. Food and Drug Administration, Press Announcements, http://www.fda.gov/NewsEvents/Newsroom/PressAnnouncements).
24. L. S. Sorkin, M. Otto, W. M. Baldwin, III, E. Vail, S. D. Gillies, R. Handgretinger, R. C. Barfield, H. M. Yu and A. L. Yu, *Pain*, 2010, **149**, 135-142.
25. L. S. Sorkin, A. L. Yu, H. Junger and C. M. Doom, *Brain Res.*, 2002, **930**, 67-74.
26. M. Görges, N. West, R. Deyell, P. Winton, W. Cheung and G. Lauder, *Pediatr. Blood Cancer*, 2015, **62**, 29-34.
27. A. L. Yu, M. M. Uttenreuther-Fischer, C. S. Huang, C. C. Tsui, S. D. Gillies, R. A. Reisfeld and F. H. Kung, *J. Clin. Oncol.*, 1998, **16**, 2169-2180.
28. ClinicalTrials.gov, 5 studies found for: Hu14.18K322A, http://clinicaltrials.gov/ct2/results?term=Hu14.18K322A&Search=Search).
29. K. L. Alderson, M. Luangrath, M. M. Elsenheimer, S. D. Gillies, F. Navid, A. L. Rakhmilevich and P. M. Sondel, *Cancer Immunol. Immun.*, 2013, **62**, 665-675.
30. F. Navid, P. M. Sondel, R. Barfield, B. L. Shulkin, R. A. Kaufman, J. A. Allay, J. Gan, P. Hutson, S. Seo, K. Kim, J. Goldberg, J. A. Hank, C. A. Billups, J. Wu, W. L. Furman, L. M. McGregor, M. Otto, S. D. Gillies, R. Handgretinger and V. M. Santana, *J. Clin. Oncol.*, 2014, **32**, 1445.
31. P. F. Jiao, H. Y. Zhou, L. X. Chen and B. Yan, *Curr. Med. Chem.*, 2011, **18**, 2086-2102.
32. A. L. Parry, N. A. Clemson, J. Ellis, S. S. R. Bernhard, B. G. Davis and N. R. Cameron, *J. Am. Chem. Soc.*, 2013, **135**, 9362-9365.
33. R. W. Childs and M. Carlsten, *Nat. Rev. Drug Discov.*, 2015, **14**, 487-498.
34. B. Duncan, C. Kim and V. M. Rotello, *J. Control. Release*, 2010, **148**, 122-127.
35. W. Jiang, Y. S. KimBetty, J. T. Rutka and C. W. ChanWarren, *Nat. Nanotech.*, 2008, **3**, 145-150.
36. P. Jiao, H. Zhou, M. Otto, Q. Mu, L. Li, G. Su, Y. Zhang, E. R. Butch, S. E. Snyder, G. Jiang and B. Yan, *J. Am. Chem. Soc.*, 2011, **133**, 13918-13921.
37. Y. Liu, M. K. Shipton, J. Ryan, E. D. Kaufman, S. Franzen and D. L. Feldheim, *Anal. Chem.*, 2007, **79**, 2221-2229.
38. J. Zhang, C. Li, X. Zhang, S. Huo, S. Jin, F.-F. An, X. Wang, X. Xue, C. I. Okeke, G. Duan, F. Guo, X. Zhang, J. Hao, P. C. Wang, J. Zhang and X.-J. Liang, *Biomaterials*, 2015, **42**, 103-111.
39. C. Peng, L. Zheng, Q. Chen, M. Shen, R. Guo, H. Wang, X. Cao, G. Zhang and X. Shi, *Biomaterials*, 2012, **33**, 1107-1119.
40. H. Wang, L. Zheng, C. Peng, M. Shen, X. Shi and G. Zhang, *Biomaterials*, 2013, **34**, 470-480.
41. E. Vivier, D. H. Raulet, A. Moretta, M. A. Caligiuri, L. Zitvogel, L. L. Lanier, W. M. Yokoyama and S. Ugolini, *Science*, 2011, **331**, 44-49.
42. E. Vivier, J. A. Nunes and F. Vely, *Science*, 2004, **306**, 1517-1519.
43. I. Tassi, J. Klesney-Tait and M. Colonna, *Immunol. Rev.*, 2006, **214**, 92-105.
44. L. L. Lanier, *Annu. Rev. Immunol.*, 1998, **16**, 359-393.
45. L. L. Lanier, *Nat. Immunol.*, 2008, **9**, 495-502.
46. D. A. Giljohann, D. S. Seferos, W. L. Daniel, M. D. Massich, P. C. Patel and C. A. Mirkin, *Angew. Chem. Int. Ed.*, 2010, **49**, 3280-3294.

Enhancing both CT imaging and natural killer cell-mediated cancer cell killing by a GD2-targeting nanoconstruct

Peifu Jiao, Mario Otto, Qiaohong Geng, Chencan Li, Faming Li, Elizabeth R. Butch, Scott E. Snyder, Hongyu Zhou and Bing Yan**